3D printing of microscopic bacterial communities

Jodi L. Connell[a,b], Eric T. Ritschdorff[a], Marvin Whiteley[b,c], and Jason B. Shear[a,c,1]

Departments of [a]Chemistry and Biochemistry and [b]Molecular Genetics and Microbiology, and [c]Institute of Cell and Molecular Biology, The University of Texas at Austin, Austin, TX 78712

Edited* by Harry L. Swinney, The University of Texas at Austin, Austin, TX, and approved September 5, 2013 (received for review May 23, 2013)

Bacteria communicate via short-range physical and chemical signals, interactions known to mediate quorum sensing, sporulation, and other adaptive phenotypes. Although most in vitro studies examine bacterial properties averaged over large populations, the levels of key molecular determinants of bacterial fitness and pathogenicity (e.g., oxygen, quorum-sensing signals) may vary over micrometer scales within small, dense cellular aggregates believed to play key roles in disease transmission. A detailed understanding of how cell–cell interactions contribute to pathogenicity in natural, complex environments will require a new level of control in constructing more relevant cellular models for assessing bacterial phenotypes. Here, we describe a microscopic three-dimensional (3D) printing strategy that enables multiple populations of bacteria to be organized within essentially any 3D geometry, including adjacent, nested, and free-floating colonies. In this laser-based lithographic technique, microscopic containers are formed around selected bacteria suspended in gelatin via focal cross-linking of polypeptide molecules. After excess reagent is removed, trapped bacteria are localized within sealed cavities formed by the cross-linked gelatin, a highly porous material that supports rapid growth of fully enclosed cellular populations and readily transmits numerous biologically active species, including polypeptides, antibiotics, and quorum-sensing signals. Using this approach, we show that a picoliter-volume aggregate of *Staphylococcus aureus* can display substantial resistance to β-lactam antibiotics by enclosure within a shell composed of *Pseudomonas aeruginosa*.

multiphoton lithography | microfabrication | antibiotic resistance | polymicrobial

Uncovering relationships between structure and function remains a central goal of biology. At molecular dimensions, protein structure can be modified to systematically evaluate how conformation gives rise to ligand binding, catalysis, and other functional properties. On the far larger scale of ecological habitats, organization plays a similarly vital role in mediating "function," where the social behavior of organisms—including their reproduction rate, mobility, and involvement in cooperative and predatory relationships—depends on the spatial arrangement of the community. As with molecular function, a detailed understanding of how organization affects behavior of communities would benefit from technologies for creating variants of defined structure.

Nowhere is the potential value of geometrical control more evident than in the study of microbial ecosystems. The burgeoning field of sociomicrobiology has revealed a richness in the mechanisms by which bacteria engage in cooperative and adversarial relationships, affecting nearby individuals through physical contact and modifications to the chemical composition of their shared microenvironment. Spatially dependent interactions can result from perturbations to the nutritional state of the local habitat, but also may be caused by release of diffusible signals and toxins, and physical protection from environmental risks afforded by aggregation. Chemical-sensing mechanisms allow bacteria to adapt gene expression to suit dynamic conditions, such as hypoxia, and to coordinate transcription of genes associated with pathogenic phenotypes, including production of virulence factors, resistance to antibiotics, and biofilm formation (1–4). Cellular and chemical landscapes can vary significantly over distances as small as several micrometers, suggesting that organization of microscopic bacterial aggregates may profoundly impact phenotypic state.

To investigate the behavior of small microbial aggregates, various microfabrication technologies have been developed that confine bacteria within microfluidic devices, microcavities, and ultralow-volume liquid droplets (5–10). Hydrogel-based materials formed from droplets are useful in maintaining and extending cell viability (11, 12) and multiple emulsion strategies have been used to produce structures such as droplets within droplets (13, 14) and some nonspheroidal geometries (15). The ability to integrate analysis systems with microfluidics has made these isolation platforms attractive for high-throughput screening applications, such as assaying antibiotic resistance (11, 12, 16) and enzymatic activity (17). Such approaches have been useful for restricting the size, shape, and physical attributes of microhabitats; none, however, has provided a means to arbitrarily define the three-dimensional (3D) geometry of bacterial aggregates or orientation of multiple populations. Moreover, the process of encapsulating cells within ultralow-volume cavities often restricts mass transport, resulting in conditions that are incompatible with growth and signaling between physically isolated populations.

We recently described a laser-writing approach, based on multiphoton lithography (MPL) (18–21), for fashioning microscopic 3D bacterial chambers from bovine serum albumin (BSA), a highly soluble protein that can be cross-linked into porous, rugged, and biocompatible hydrogels (22, 23). Using these bacterial "lobster traps," individual motile bacteria were confined after entering picoliter-sized BSA chambers and could be grown into clonal populations at rates indistinguishable from those observed in batch culture (22). Facile diffusion of biologically relevant molecules through the BSA walls, including

Significance

Bacteria within the human body commonly thrive within structured three-dimensional (3D) communities composed of multiple bacterial species. Organization of individuals and populations within bacterial aggregates is believed to play key roles in mediating community attributes, affecting, for example, the virulence of infections within the cystic fibrosis lung and oral cavity. To gain detailed insights into how geometry may influence pathogenicity, we describe a strategy for 3D printing bacterial communities in which physically distinct but chemically interactive populations of defined size, shape, and density can be organized into essentially any arrangement. Using this approach, we show that resistance of one pathogenic species to an antibiotic can enhance the resistance of a second species by virtue of their 3D relationship.

Author contributions: J.L.C., E.T.R., M.W., and J.B.S. designed research; J.L.C. and E.T.R. performed research; J.L.C., E.T.R., M.W., and J.B.S. analyzed data; and J.L.C., E.T.R., M.W., and J.B.S. wrote the paper.

The authors declare no conflict of interest.

*This Direct Submission article had a prearranged editor.

[1]To whom correspondence should be addressed. E-mail: jshear@mail.utexas.edu.

This article contains supporting information online at www.pnas.org/lookup/suppl/doi:10.1073/pnas.1309729110/-/DCSupplemental.

quorum-sensing signals and antibiotics, provided a means to investigate how bacterial social behaviors depend on population size and density, container shape, and flow rate of the surrounding medium.

Despite these advantages, the need for bacteria to transit from bulk medium into microchambers severely limits the utility of this approach for organizing complex communities of cells composed of physically segregated but chemically communicative populations. In principle, natural bacterial motility could be exploited to construct many bacterial arrangements. Unfortunately, when models require that multiple bacterial species be distributed to specific compartments at desired densities, random motion proves to be a highly inefficient approach for assembling communities. Moreover, numerous configurations of interest, such as polymicrobial communities containing immotile bacterial and nested geometries in which a cellular microcluster is surrounded on all sides by a distinct population, could not be created using motility to distribute cells into prefabricated traps.

As an alternative, one could consider constructing containers using in situ lithography. We and others have previously shown MPL can be used to fabricate a variety of surface-attached features in the presence of both eukaryotic and prokaryotic cells, although survivability has been poor and the fabrication methods did not offer a means to organize multiple populations with arbitrary 3D control (24–26).

Here, we report a micro-3D printing strategy for creating "designer" ecosystems tailored to investigate the interaction and integration of multiple bacterial populations within essentially any 3D arrangement. In this approach, bacteria are mixed into a warm (37 °C) fabrication solution composed of gelatin and a photosensitizing molecule that promotes chemical cross-linking of polypeptides following photoexcitation. This technique, based on direct cross-linking of unmodified gelatin as opposed to less biocompatible chemistry [e.g., using methacrylated polypeptides (27–29)] is key to maintaining cell viability. By allowing the mixture to cool to ambient temperatures, bacteria become suspended at various 3D positions throughout the thermally set gel. Enclosures of specified geometry are fabricated around one or more bacteria by scanning a tightly focused pulsed laser beam in three dimensions. Nonlinear dependence of photosensitizer excitation on laser intensity restricts protein photo–cross-linking to diffraction-limited fabrication voxels centered around the laser focus (19), providing the ability to print populations of bacteria with submicrometer 3D resolution. Moreover, the mechanical and chemical properties of printed structures can be tuned by adding desired proteins, such as BSA, to the fabrication gel. Communities containing multiple populations of segregated bacteria can be produced by mixing two or more bacterial species in a single fabrication gel, or by printing different cell types sequentially using multiple fabrication gels.

Using this approach, we demonstrate the ability to nest distinct microbial populations in core–shell arrangements, including aggregates of a single species at vastly differing densities, and polymicrobial communities containing motile and nonmotile bacteria. We show that spatially localized interactions between Gram-positive *Staphylococcus aureus* and Gram-negative *Pseudomonas aeruginosa*—two human pathogens that often form persistent coinfections within wounds, catheters, and the lungs of cystic fibrosis patients—enhance survival of *S. aureus* during treatment with a β-lactam antibiotic.

Results and Discussion

Physically sealed but porous protein microstructures are formed around both suspended and settled bacteria via micro-3D printing. In this approach—based on MPL—protein reagent is photo–cross-linked within a reaction voxel that can be scanned to build extended 3D shapes with submicron resolution (19). Reaction voxels are created by focusing pulsed laser light using high-numerical aperture optics, an approach that establishes focal intensities great enough to excite electronic transitions through the concerted absorption of multiple low-energy photons. In the current studies, excitation of either methylene blue or Rose Bengal yields singlet oxygen with high efficiency, which subsequently promotes intramolecular and intermolecular covalent cross-linking reactions between both BSA and gelatin.

Gelatin is a polydisperse mixture of high–molecular-weight protein fragments produced by partial hydrolysis of collagens, related structural proteins notable for their high levels of the integrin-binding sequence, RGD. Below temperatures of ~35 °C, gelatin solutions undergo reversible gelation (30), forming a high-water content, porous matrix that retains some favorable cellular interactions characteristic of native collagen. The unique physical and chemical properties of this biomaterial have motivated interest in using gelatin as an embedding medium in a range of cellular applications, including storage (31), immobilization (32), and 3D culturing (33) of bacteria.

The basic steps of 3D cellular printing are shown in Fig. 1*A*. In brief, bacterial cells are diluted and mixed into a fabrication precursor containing gelatin, BSA (to enhance mechanical properties), and photosensitizer. A droplet of this cellular suspension is transferred to a sterile sample well at 37 °C, then cooled to ambient temperature (18–22 °C) to form a gelled reagent containing bacteria suspended throughout the matrix. MPL is used to print fully enclosed microcontainers of desired shape around individual or small groups of cells at specified 3D coordinates within the gel. Nascent microstructures undergo negligible drift when fabrication is performed within this gelatin-based reagent, making it possible to create both surface-adherent and free-floating microcontainers unanchored to an immobile surface. In this way, bacteria can be organized into true core–shell geometries, with the internal core fully encompassed by a physically segregated shell population. Following fabrication, excess precursor is removed by rinsing the sample well using warm media, such as tryptic soy broth (TSB), a process that melts remaining gel to leave bacteria free to move within media-filled microfabricated chambers. In the case of surface-adherent boxes, such chambers would thus be defined by walls and a roof comprised of cross-linked gelatin/BSA, and a coverglass floor.

Unlike materials produced using conventional photolithography, gelatin-based barriers fabricated using micro-3D printing are highly permeable to a range of chemical species, including unreacted precursor initially located within the cavity of cellular microcontainers and metabolic waste products generated during cell growth. As a consequence, the microenvironment within sealed microcontainers is capable of supporting proliferation for >90% of *P. aeruginosa* and *S. aureus* cells following micro-3D printing, with approximate doubling times of 45 and 34 min., respectively, at 37 °C.

Gelatin-based MPL provides an in situ microfabrication platform in which small groups of bacteria can be arranged in an essentially unlimited range of 3D geometries. To assess the utility of this 3D-printing approach for growing bacterial monocultures within sealed microcavities, individual *P. aeruginosa* cells are confined within basic geometrical shapes: an anchored pyramid and an untethered torus retained at the surface using a flat-headed pin (Fig. 1*B* and Fig. S1). Both cells undergo rapid division over the course of many hours, illustrating that the encapsulation process does not compromise viability.

Bacteria embedded in a thermally set gelatin precursor are dispersed in three dimensions, allowing multiple populations of cells to be printed in complex configurations that can have definable chemical and physical interconnectivity. For example, the multicompartmental structure shown in Fig. 1*C* is composed of six spheroidal *P. aeruginosa* microcolonies of differing size, all of which are physically segregated (and anchored to the glass via two cylindrical posts). Chemical interactions between these

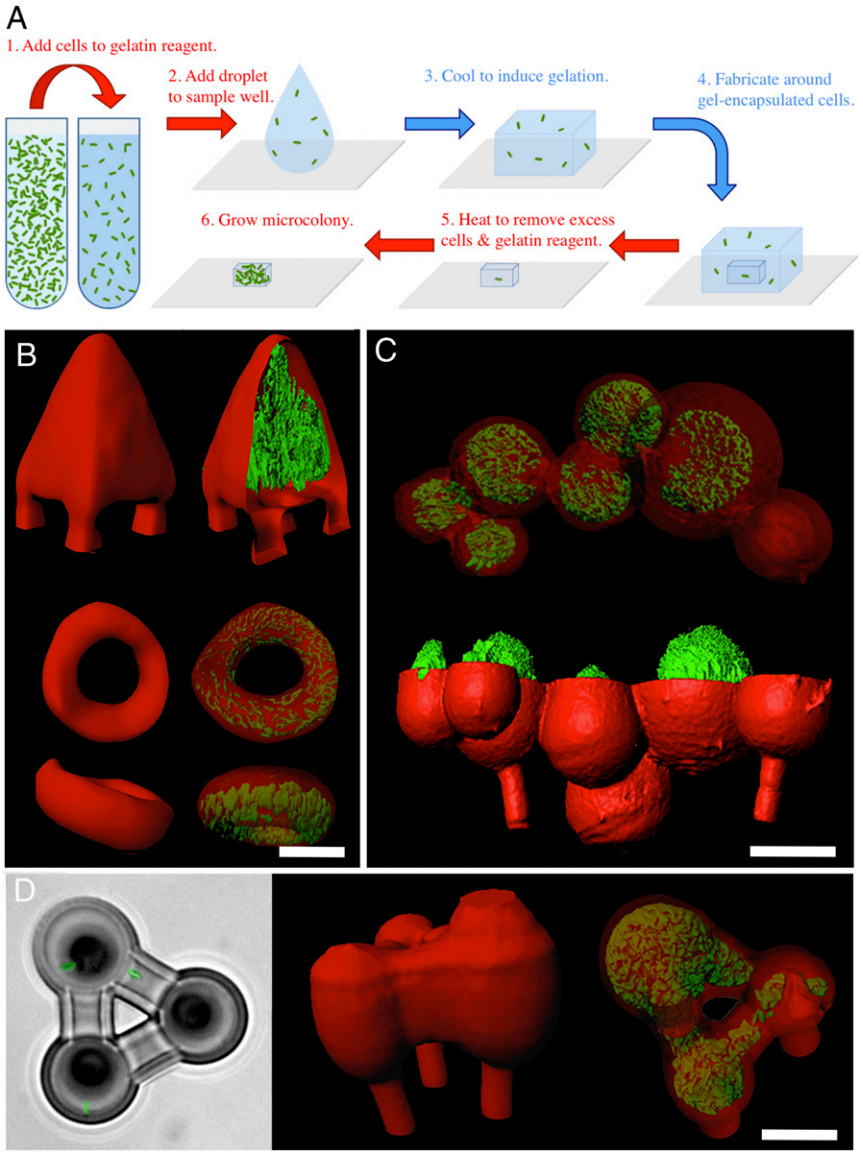

Fig. 1. Gelatin-based micro-3D printing in the presence of bacteria. (*A*) Schematic depicting in situ microfabrication around cells encapsulated in thermally set gelatin. The red and blue arrows indicate steps performed at 37 °C or 18–22 °C, respectively. (*B*) Confocal fluorescence isosurfaces show isolated *Pseudomonas aeruginosa* microcolonies within a surface-anchored 2-pL pyramid (*Top*; two cells initially) and an untethered 3-pL torus (*Bottom*; partially transparent on the right views; one cell initially; see also Fig. S1). (*C*) Partially transparent and cut-out views of confocal fluorescence isosurfaces illustrate six physically segregated *P. aeruginosa* populations organized in three dimensions within a series of spheroid cavities (2–15 pL in volume) tethered to the glass surface by two cylindrical posts, where the right-most spheroid is vacant and the others initially contained either one or two cells. A side view of these clusters is shown in the lower image in which the upper portion of the red channel is digitally removed to reveal bacterial clusters. The upper image provides a top-down view of the same community, with the transparency of the red channel adjusted to reveal bacterial clusters. (*D*) A bright-field image acquired 10 min postfabrication (*Left*), and side-on and partially transparent top-down views of a confocal fluorescence isosurface (*Center* and *Right*, respectively) showing colony growth at 18 h. The spheroidal chambers are physically connected by channels such that motile *P. aeruginosa* cells can distribute throughout the 5-pL structure according to preference. Cylindrical posts extend from the base of each spheroid to tether the structure to the glass surface. See also Fig. S2. Cells are false-colored green in *B*–*D* for visualization. (Scale bars, 20 μm.)

populations should vary, however, depending on the relative position of an enclosure and the degree to which its porous walls are shared with adjacent populations. Alternatively, Fig. 1*D* depicts a complex microenvironment suitable for characterizing interactions between multiple populations with the potential for dynamic spatial organization. In this example, individual *P. aeruginosa* cells are initially arranged in three surface-tethered microspheroids such that the motile bacteria are free to migrate throughout the entire structure once the excess gelatin reagent is removed. Here, *P. aeruginosa* colonizes one of the spheroidal chambers more rapidly than the two additional chambers and three channels, causing substantial expansion of this initial chamber after several hours (Fig. 1*D* and Fig. S2). Preferential colonization of *P. aeruginosa* was observed in some (but not all) microstructures; this trend was consistent in multiple replicate experiments.

Organizing cells within unanchored microcontainers provides opportunities both for nesting distinct cell types/densities, and for dynamically altering the orientation of entire bacterial populations within a community. These concepts are shown in Fig. 2, in which a small (1 pL), high-density (hundreds of cells per picoliter) population of *P. aeruginosa* samples the confines of a larger box (~55 pL; the 5-μm-thick roof is optically transparent in the image series shown in Fig. 2) containing *P. aeruginosa* at low density (~5–10 cells·pL^{-1}) of the same cell type. The image series acquired after ~6 h of growth at 37 °C shows that the population within the spherical chamber (initially one cell) has reached a high enough density due to cell growth to render the bacteria immobile, whereas collisions with the lower density *P. aeruginosa* cells in the larger, fully enclosed, surface-attached box cause the free-floating sphere to move and rotate throughout the chamber in three dimensions (Movie S1). Although the changing relative orientation of the two populations is caused by apparently random motion of the free-swimming bacteria, the free-floating arrangement of bacterial microclusters also can be manipulated to desired spatial arrangements using optical tweezers.

The true power of 3D cellular printing is evident in its capabilities for arranging polymicrobial communities in an essentially unlimited assortment of geometries. Because bacteria in natural environments rarely reside as monocultures, application of this approach to polymicrobial communities is of particular significance. *S. aureus* and *P. aeruginosa* are two opportunistic human pathogens that coinfect various clinically relevant environments, including the lungs of cystic fibrosis patients and chronic wounds.

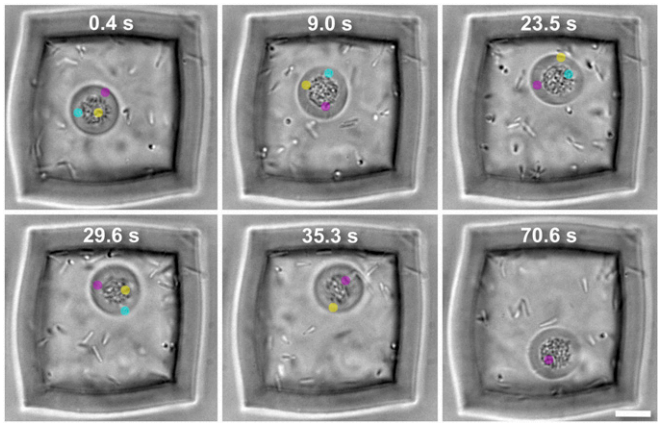

Fig. 2. Nesting of a mobile bacterial microcluster within a physically isolated population. The 70-s sequence shows a time series acquired ~6 h postfabrication in which a tightly packed, 1-pL spheroidal population (initially one cell) of *P. aeruginosa* is buffeted by freely swimming *P. aeruginosa* contained within an exterior 55-pL "shell" (initially two cells; see also Movie S1). The 5-μm-thick roof on the exterior shell is optically transparent and not visible in the images. The green, pink, and yellow reference markers show the rotation of the sphere in three dimensions. (Scale bar, 10 μm.)

Fig. 3 illustrates the use of 3D cellular printing for engineering spatially defined communities of *S. aureus* and *P. aeruginosa* cocultures. The growth of a simple mixed-species population in an enclosed microcontainer is shown in Fig. 3*A*. Here, images are acquired over a 10-h incubation period at 37 °C, revealing that both *S. aureus* and *P. aeruginosa* remain viable and grow within the confined coculture (Movie S2). This result displays that possible effects from extracellular factors (e.g., from pyocyanin, a *P. aeruginosa*-produced antimicrobial) is not a significant factor in cell death. The relatively low stiffness of the gelatin–BSA matrix allows the walls and 2-μm-thick roof of the container to distend dramatically to accommodate growth of the mixed population.

Spatial structure is likely to contribute to the phenotype within polymicrobial communities in many natural environments, such as dental plaque and the cystic fibrosis lung. Various strategies have emerged to investigate this concept within a limited range of geometries by using microfluidic devices to create defined patterns of different species in separate wells sharing a common communication channel (34) and extruding multiple suspensions of bacterial cells together into a core–shell fiber (35). We explored the capacity to construct different complex geometries for arranging polymicrobial communities by sequentially printing 3D bacterial microcolonies, first an anchored core containing *S. aureus*, then a surrounding shell inhabited by *P. aeruginosa* (Fig. 3*B* and Fig. S3). The 3D mask reconstructions show the porous, cross-linked walls and roof of the nested (pink) and exterior (green) chambers used to organize the bacteria in physically segregated, polymicrobial communities (Fig. 3*B*, *Upper*). By varying the density of the cells added to the fabrication precursor in each fabrication step or allowing confined *S. aureus* to grow between fabrication steps, it is possible to control the resultant cell density for each species independently while retaining high chemical connectivity via a nested geometry. These concepts, as well as the flexibility this fabrication strategy offers to customize the confinement geometry, are both demonstrated in Fig. 3*B*, by arbitrarily using a cube (*Left*) and a hemisphere (*Right*) for organizing the nested communities.

Precisely defined polymicrobial geometries make it possible to study the role of organization on cell–cell interactions at a level not previously attainable. In earlier studies that used "lobster trap" chambers to catch bacteria, we investigated how the number and density of *P. aeruginosa* within a single, well-defined microcluster affected phenotypic resistance to antibiotic toxicity. Micro-3D printing of cells fundamentally extends these abilities, opening possibilities for probing how the antibiotic resistance of one bacterial microcluster may influence the antibiotic susceptibility of adjacent, surrounding, or embedded populations—a question of particular relevance to infections at various in vivo sites (e.g., wounds, the oral cavity, the cystic fibrosis lung) where tissue is often co-colonized by multiple bacterial species.

Here, we hypothesized that *S. aureus*, a bacterium naturally susceptible to the action of β-lactam–based antibiotics, would be sheltered from ampicillin toxicity when embedded within a microcolony of *P. aeruginosa* actively producing β-lactamases. After 3D printing of several *S. aureus* cells surrounded by a shell containing one or two *P. aeruginosa* cells (sealed by a 5-μm-thick roof and a coverglass floor; Fig. 4*A* and Fig. S3), microcolonies were grown for several hours then subjected to ampicillin for 2 h at

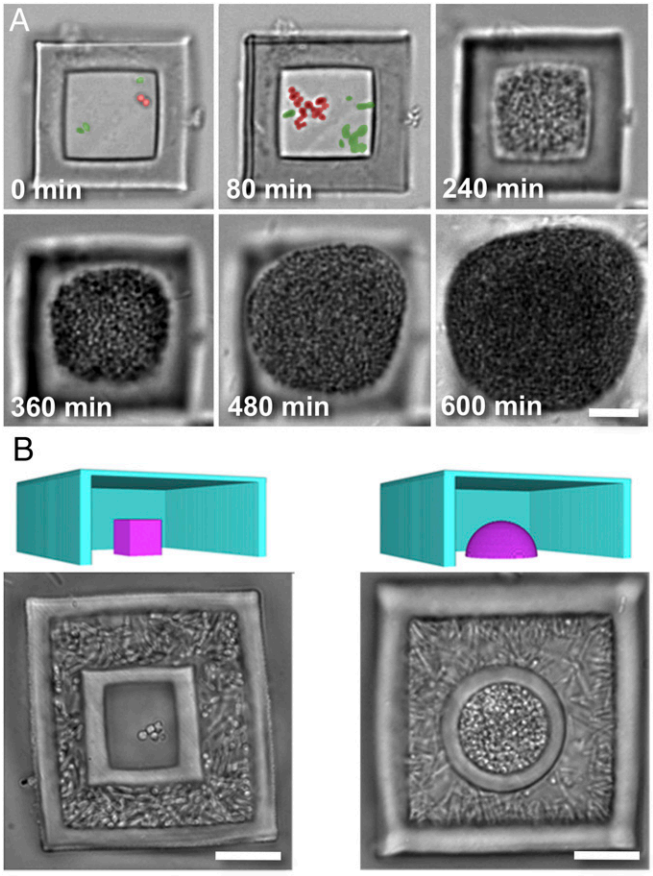

Fig. 3. Engineering polymicrobial communities. (*A*) *Staphylococcus aureus* and *P. aeruginosa* cells are embedded in one precursor gel to form a physically mixed polymicrobial community. Bright-field images acquired at 37 °C over 10 h show growth of the mixed colony, with the enclosure (initially 8 pL) roof and walls distending dramatically over the last several hours of growth (Movie S2). Eventually, the structure's 2-μm-thick roof ruptured, releasing cells into the surrounding medium (not shown). *S. aureus* and *P. aeruginosa* cells are false-colored red and green, respectively, for visualization in the "0 min" and "80 min" images. (*B*) Cut-away 3D mask reconstructions (*Upper*) and bright-field images (*Lower*) depict examples of nested polymicrobial communities of varying geometries and cell densities (see also Fig. S3). Low-density (*Left*) and high-density (*Right*) *S. aureus* microclusters are confined in rectangular and hemispherical cavities, respectively, surrounded by high-density *P. aeruginosa* populations. Inner cavities are 1 pL and outer chambers are 30 pL. The 5-μm-thick roofs used to seal in inner cavities and the outer chambers are not visible in the bright-field images. (Scale bars, 10 μm.)

the minimum inhibitory concentration (MIC) for *S. aureus* (0.15 $\mu g \cdot mL^{-1}$).

In these defined communities, we observed that a localized shell of *P. aeruginosa* afforded substantial protection to encapsulated *S. aureus* microcolonies from ampicillin (Fig. 4*B*, *Right*) relative to confined *S. aureus* microcolonies dosed in monoculture (Fig. 4*B*, *Left*). When 3D printing cocultures, some *P. aeruginosa* cells remained outside gelatin structures following extensive washing. To assess the degree of protection afforded by the resultant population of dispersed *P. aeruginosa*, we also determined ampicillin susceptibility of *S. aureus* microcolonies in a similar environment that lacked the localized *P. aeruginosa* shell (Fig. 4*B*, *Left*). Although dispersed *P. aeruginosa* alone was found to improve *S. aureus* survival, localized shells offered more benefit. Moreover, in monoculture and coculture, surrounding *S. aureus* with an empty shell did not affect survival.

Greater levels of protection are provided by *P. aeruginosa* that produce more β-lactamase. Microclusters of *S. aureus* were surrounded by two different *P. aeruginosa* PAO1 strains: wild-type [PAO1 (WT)] (MIC_{amp} = 160 $\mu g \cdot mL^{-1}$) and PAO1 carrying a plasmid (pMRP9-1) that confers greatly enhanced resistance to β-lactams [PAO1 (β-lac^R)] (MIC_{amp} = 10,280 $\mu g \cdot mL^{-1}$). We found that PAO1 (β-lac^R) offered ∼1.6-fold more localized protection of *S. aureus* from ampicillin in comparison with the wild-type strain (dark gray and light gray bars, respectively; Fig. 4*B*, *Right*).

We found that *S. aureus* at a broad range of densities was afforded protection from ampicillin by *P. aeruginosa* shells. *S. aureus* cores containing as few as 6 cells and as many as 207 cells in 4-pL volumes displayed 80% survival when surrounded by shells of PAO1 (β-lac^R) (compared with a 40% survival rate without shells; Fig. 4*B*, *Right*). Moreover, even relatively low-density shells of PAO1 (β-lac^R) were able to dramatically decrease the susceptibility of *S. aureus* to ampicillin. Again, a survival rate of ∼80% was achieved both when an *S. aureus* population was surrounded by a shell containing less than 2 cells·pL^{-1} (120 live cells in a 72-pL shell) of PAO1 (β-lac^R) and for a shell containing 50 cells·pL^{-1} (1,000 live cells in 20 pL). These results suggest that relatively low densities of PAO1 (β-lac^R) can effectively degrade ampicillin as it diffuses toward the *S. aureus* core, perhaps aided by release of β-lactamase within vesicular membranes (36–38).

Although we and others previously have demonstrated that MPL can be performed in the presence of living cells that have settled to the surface of a substrate (25, 26), the micro-3D printing strategy described here provides capabilities for creating complex communities of organisms arranged with micrometer resolution in essentially any 3D geometry. The primary drawback associated with this method is the relatively high cost of the specialized equipment required for micro-3D printing. In addition, the direct-write nature of this 3D printing process suggests that, at present, this technique is not well suited for high-throughput analyses. Nevertheless, because microstructure geometries often can be taken from concept to printing within as little as several minutes, it offers an attractive means to perform rapid prototyping of different 3D arrangements. Bacterial microcolonies can be organized either with well-specified or dynamic orientations, providing a powerful platform to begin to unravel how numerous social behaviors—including resource competition, symbiosis, and population-dependent antibiotic resistance—may originate within communities composed of microscopic clusters of cells. Key to this strategy is the use of thermally set gelatin mixtures as a reagent for micro-3D printing, which provides the ability to print enclosures around any bacterial cell of interest suspended within the hydrogel matrix. This versatile fabrication strategy presents a foundation to explore the elaborate mechanisms that allow bacteria to adapt and thrive in complex, heterogeneous environments in nature.

Micro-3D printing should be a valuable tool for examining mechanisms and dynamics of adaptive responses to environmental conditions. Unanchored microcolonies that have grown to targeted densities or after exposure to sublethal doses of an antibiotic could be harvested and subjected to transcriptomic and metabolomic analyses. Moreover, this fabrication approach could be used to seed defined bacterial microcolonies in animal hosts to study how infections develop in vivo. Nesting a bacterial colony within a higher or lower density community, such that it is completely surrounded in three dimensions (either by the same or different species), could provide insights into the underlying mechanisms involved in cellular communication and the onset of social behaviors between microbes within proximity to one another.

Materials and Methods

Materials. Details are provided in *SI Materials and Methods*.

Bacterial Strains and Cell Culture. Wild-type *P. aeurginosa* strain PAO1, *P. aeruginosa* PAO1 constitutively expressing GFP from the plasmid pMRP9-1 (39), and *S. aureus* MN8 carrying the *sar* P1 reporter plasmid pJY209 with yfp_{10B} (40) were used in these studies. *S. aureus* cells were conditioned to become acclimated to methylene blue before fabrication. Details regarding *S. aureus* conditioning and incorporation of bacteria into fabrication solutions are provided in *SI Materials and Methods*.

Gelatin-Based Micro-3D Printing. Photo–cross-linked protein microstructures were fabricated on the untreated surface within a 0.8-mL well of a Lab-Tek

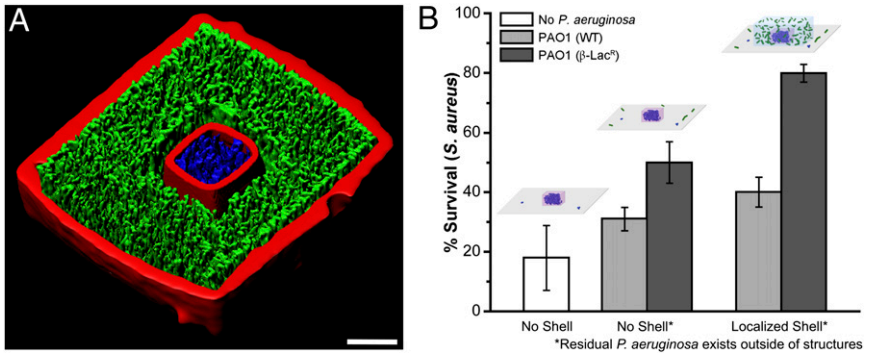

Fig. 4. Sharing of antibiotic resistance within a polymicrobial community containing *P. aeruginosa* and *S. aureus*. (*A*) Cut-away view of a confocal fluorescence isosurface revealing a nested *S. aureus* microcolony surrounded by *P. aeruginosa* on all sides except for the coverglass surface (see also Fig. S3; scale bar, 10 μm). (*B*) Confined microcolonies of *S. aureus* display resistance to ampicillin via the action of cocultured *P. aeruginosa*. Monocultures of *S. aureus* experience approximately an 80% kill rate when exposed to ampicillin at the MIC for 2 h (white bar, *Left*). Confined *S. aureus* with residual *P. aeruginosa* in the surrounding growth medium exhibits some resistance to the β-lactam antibiotic (*Center*). Survival of *S. aureus* is significantly enhanced when confined microclusters are nested within high-density populations of *P. aeruginosa* (*Right*). Additionally, PAO1 that overproduces β-lactamase [PAO1 (β-Lac^R); dark gray bars] provides enhanced protection from ampicillin relative to PAO1 wild-type [PAO1 (WT); light gray bars]. (*Inset*) Schematics depicting the three different dosing conditions. *S. aureus* and *P. aeruginosa* cells appear blue and green, respectively. *S. aureus* microcolonies initially contained two to eight cells within a 1- to 4-pL cavity. Nested populations are surrounded by 10- to 20-μm-thick layer of *P. aeruginosa* in the *x*–*y* dimensions that extends 15–50 μm in the *z* dimension (shell volumes ranged between 20 and 150 pL). Error bars represent 1 SD between individual microstructures containing *S. aureus* ($n \geq 4$) pooled from multiple biological replicates ($N_{Bio} \geq 2$).

chambered #1 coverglass using a dynamic mask-directed multiphoton lithography technique described in detail elsewhere (19, 41). In brief, galvanometer-driven scan mirrors (GVS002; Thor Labs) were used to raster-scan the focused 740-nm output from a mode-locked titanium:sapphire (Ti:S) laser (Tsunami; Spectra Physics) across the reflective face of a digital micromirror device (DMD) (SVGA), which served as a dynamic mask. The reflected Ti:S beam was collimated and directed to overfill ($1/e^2$) the back aperture of an oil-immersion objective (an Olympus UPlanApo 100×, 1.35 N.A., or an Olympus PlanApo 60×, 1.40 N.A.) positioned on an inverted microscope (Zeiss; Axiovert).

Binary mask sequences that were used to create micro–3D-printed structures were created using Adobe Photoshop or the ImageJ macro language (http://rsbweb.nih.gov/ij/developer/macro/macros.html; ImageJ, version 1.44o, by Wayne Rasband, National Institutes of Health, Bethesda, MD). All 3D microforms in this work were printed at 3.3 s per plane in a layer-by-layer process by synchronizing binary mask presentation on the DMD with 0.50-μm optical axis steps controlled by a motorized focus driver (H122; Prior Scientific). The time required to print an individual microstructure ranged from 1 to 6 min, depending on microstructure height.

Microstructures were fabricated in situ to confine midlogarithmic-phase bacteria embedded in a thermally set gel. Bacteria were initially diluted 1:10 into a fabrication precursor and mixed thoroughly at 37 °C. The final concentration of the fabrication solution was 300 mg·mL^{-1} gelatin (type A), 25 mg·mL^{-1} BSA, and either 2.5–8.5 mM Rose Bengal or 5.0 mM methylene blue prepared in TSB. A ∼50-μL droplet of this solution containing bacteria was transferred to a sample well at 37 °C. After 1–2 min at ambient temperature (18–22 °C), the droplet formed a gel, which temporarily immobilized the cells. Microstructures were fabricated around the embedded bacteria (1 or 2 *P. aeruginosa* cells, or clusters containing 2–10 *S. aureus* cells) using an average laser power of ∼75 mW (measured at the back aperture of the objective). After fabrication, the un–cross-linked gelatin/BSA was washed out of the sample well using multiple volumes (∼0.5 mL per wash) of 37 °C TSB. The sample was incubated at 37 °C and washed with fresh TSB periodically for the remainder of the experiment (Fig. 1*A*).

β-Lactam Susceptibility in Polymicrobial Populations. To ensure that the bacteria were dividing in these studies, confined *S. aureus* cells were grown for 4 h in TSB at 37 °C before printing an exterior shell of *P. aeruginosa* around the inner cavities. The two species were grown in coculture for 2 h at 37 °C, then left at ambient temperature for 12 h (overnight). The following day, samples were washed using fresh TSB and returned to 37 °C. After an additional 4 h of growth at 37 °C, the polymicrobial samples were dosed using the MIC of ampicillin determined for the methylene blue-conditioned *S. aureus* cells (0.15 μg·mL^{-1}) for 2-h period at 37 °C (Fig. S2). Following the antibiotic dose, survival was assessed by staining cells using a Live/Dead BacLight viability kit, which allowed live and dead to be visualized in the green and red channels, respectively, using either wide-field fluorescence or confocal microscopy.

Imaging and Data Analysis. Details of bright-field, wide-field fluorescence, and confocal fluorescence imaging are provided in *SI Materials and Methods*.

ACKNOWLEDGMENTS. We gratefully acknowledge experimental assistance from Tim Hooper. J.B.S. and M.W. are Fellows of the Institute for Cellular and Molecular Biology. This work was supported by National Institutes of Health Grant 5R21AI097929-02 and The Robert A. Welch Foundation Grant F-1331.

1. Parsek MR, Greenberg EP (2005) Sociomicrobiology: The connections between quorum sensing and biofilms. *Trends Microbiol* 13(1):27–33.
2. Horswill AR, Stoodley P, Stewart PS, Parsek MR (2007) The effect of the chemical, biological, and physical environment on quorum sensing in structured microbial communities. *Anal Bioanal Chem* 387(2):371–380.
3. Balaban NQ, Merrin J, Chait R, Kowalik L, Leibler S (2004) Bacterial persistence as a phenotypic switch. *Science* 305(5690):1622–1625.
4. Hall-Stoodley L, Stoodley P (2005) Biofilm formation and dispersal and the transmission of human pathogens. *Trends Microbiol* 13(1):7–10.
5. Boedicker JQ, Vincent ME, Ismagilov RF (2009) Microfluidic confinement of single cells of bacteria in small volumes initiates high-density behavior of quorum sensing and growth and reveals its variability. *Angew Chem Int Ed Engl* 48(32):5908–5911.
6. Flickinger ST, et al. (2011) Quorum sensing between *Pseudomonas aeruginosa* biofilms accelerates cell growth. *J Am Chem Soc* 133(15):5966–5975.
7. Carnes EC, et al. (2010) Confinement-induced quorum sensing of individual *Staphylococcus aureus* bacteria. *Nat Chem Biol* 6(1):41–45.
8. Cho HJ, et al. (2007) Self-organization in high-density bacterial colonies: Efficient crowd control. *PLoS Biol* 5(11):e302.
9. Yaguchi T, et al. (2012) Aqueous two-phase system-derived biofilms for bacterial interaction studies. *Biomacromolecules* 13(9):2655–2661.
10. Volfson D, Cookson S, Hasty J, Tsimring LS (2008) Biomechanical ordering of dense cell populations. *Proc Natl Acad Sci USA* 105(40):15346–15351.
11. Eun YJ, Utada AS, Copeland MF, Takeuchi S, Weibel DB (2011) Encapsulating bacteria in agarose microparticles using microfluidics for high-throughput cell analysis and isolation. *ACS Chem Biol* 6(3):260–266.
12. Guo MT, Rotem A, Heyman JA, Weitz DA (2012) Droplet microfluidics for high-throughput biological assays. *Lab Chip* 12(12):2146–2155.
13. Shah RK, et al. (2008) Designer emulsions using microfluidics. *Mater Today* 11(4):18–27.
14. Wang W, et al. (2011) Controllable microfluidic production of multicomponent multiple emulsions. *Lab Chip* 11(9):1587–1592.
15. Shum HC, et al. (2010) Droplet microfluidics for fabrication of non-spherical particles. *Macromol Rapid Commun* 31(2):108–118.
16. Boedicker JQ, Li L, Kline TR, Ismagilov RF (2008) Detecting bacteria and determining their susceptibility to antibiotics by stochastic confinement in nanoliter droplets using plug-based microfluidics. *Lab Chip* 8(8):1265–1272.
17. Baret JC, et al. (2009) Fluorescence-activated droplet sorting (FADS): Efficient microfluidic cell sorting based on enzymatic activity. *Lab Chip* 9(13):1850–1858.
18. Li LJ, Fourkas JT (2007) Multiphoton polymerization. *Mater Today* 10(6):30–37.
19. Nielson R, Kaehr B, Shear JB (2009) Microreplication and design of biological architectures using dynamic-mask multiphoton lithography. *Small* 5(1):120–125.
20. Kawata S, Sun HB, Tanaka T, Takada K (2001) Finer features for functional microdevices. *Nature* 412(6848):697–698.
21. Kim D, So PTC (2010) High-throughput three-dimensional lithographic microfabrication. *Opt Lett* 35(10):1602–1604.
22. Connell JL, et al. (2010) Probing prokaryotic social behaviors with bacterial "lobster traps." *mBio* 1(4):e00202–e00210.
23. Connell JL, Whiteley M, Shear JB (2012) Sociomicrobiology in engineered landscapes. *Nat Chem Biol* 8(1):10–13.
24. Kaehr B, Allen R, Javier DJ, Currie J, Shear JB (2004) Guiding neuronal development with in situ microfabrication. *Proc Natl Acad Sci USA* 101(46):16104–16108.
25. Kaehr B, Shear JB (2009) High-throughput design of microfluidics based on directed bacterial motility. *Lab Chip* 9(18):2632–2637.
26. Harper JC, Brozik SM, Brinker CJ, Kaehr B (2012) Biocompatible microfabrication of 3D isolation chambers for targeted confinement of individual cells and their progeny. *Anal Chem* 84(21):8985–8989.
27. Ovsianikov A, et al. (2011) Laser fabrication of three-dimensional CAD scaffolds from photosensitive gelatin for applications in tissue engineering. *Biomacromolecules* 12(4):851–858.
28. Ovsianikov A, et al. (2011) Laser fabrication of 3D gelatin scaffolds for the generation of bioartificial tissues. *Materials* 4(1):288–299.
29. Engelhardt S, et al. (2011) Fabrication of 2D protein microstructures and 3D polymer-protein hybrid microstructures by two-photon polymerization. *Biofabrication* 3(2):025003.
30. Ward AG (1977) *The Science and Technology of Gelatin* (Academic, New York).
31. Obara Y, Yamai S, Nikkawa T, Shimoda Y, Miyamoto Y (1981) Preservation and transportation of bacteria by a simple gelatin disk method. *J Clin Microbiol* 14(1):61–66.
32. Kailas L, et al. (2009) Immobilizing live bacteria for AFM imaging of cellular processes. *Ultramicroscopy* 109(7):775–780.
33. Jordan P, et al. (2005) Creating permanent 3D arrangements of isolated cells using holographic optical tweezers. *Lab Chip* 5(11):1224–1228.
34. Kim HJ, Boedicker JQ, Choi JW, Ismagilov RF (2008) Defined spatial structure stabilizes a synthetic multispecies bacterial community. *Proc Natl Acad Sci USA* 105(47):18188–18193.
35. Kim HJ, Du W, Ismagilov RF (2011) Complex function by design using spatially pre-structured synthetic microbial communities: Degradation of pentachlorophenol in the presence of Hg(ii). *Integr Biol (Camb)* 3(2):126–133.
36. Bomberger JM, et al. (2009) Long-distance delivery of bacterial virulence factors by *Pseudomonas aeruginosa* outer membrane vesicles. *PLoS Pathog* 5(4):e1000382.
37. Ciofu O, Beveridge TJ, Kadurugamuwa J, Walther-Rasmussen J, Høiby N (2000) Chromosomal beta-lactamase is packaged into membrane vesicles and secreted from *Pseudomonas aeruginosa*. *J Antimicrob Chemother* 45(1):9–13.
38. Hunter RC, Beveridge TJ (2005) High-resolution visualization of *Pseudomonas aeruginosa* PAO1 biofilms by freeze-substitution transmission electron microscopy. *J Bacteriol* 187(22):7619–7630.
39. Davies DG, et al. (1998) The involvement of cell-to-cell signals in the development of a bacterial biofilm. *Science* 280(5361):295–298.
40. Yarwood JM, Bartels DJ, Volper EM, Greenberg EP (2004) Quorum sensing in *Staphylococcus aureus* biofilms. *J Bacteriol* 186(6):1838–1850.
41. Ritschdorff ET, Nielson R, Shear JB (2012) Multi-focal multiphoton lithography. *Lab Chip* 12(5):867–871.